"SANDIEGO"

1164-33

RADIAL METROLOGY WITH A PANORAMIC ANNULAR LENS

by

Donald R. Matthys
Physics Dept.
Marquette University
Milwaukee, WI 53233

Pal Greguss
Applied Biophysics Lab
Technical Univ. of Budapest
Budapest, Hungary H-1502

John A. Gilbert David L. Lehner Amy S. Kransteuber
Department of Mechanical Engineering
University of Alabama in Huntsville
Huntsville, AL 35899

Abstract

In the present paper, cavity shapes are profiled using two opposing collinear panoramic annular lenses. A speckle pattern is projected out from one panoramic annular lens onto a reference standard or onto the cavity wall itself, and the resulting speckle distribution is recorded through the second panoramic annular lens. Since the speckle pattern moves as the shape of the cavity changes, the variation in cavity shape can be measured by applying correlation techniques to the speckle patterns obtained before and after the cavity shape is modified. The apparent speckle movement is computed by numerically correlating small subsets extracted from each pattern. These shifts are used to measure surface deflections or to contour the cavity with respect to a reference shape.

Introduction

Radial metrology is a process devised to study the inner surfaces of cavities found, for example, inside pipes, tubes, and boreholes, using a unique panoramic annular lens[1] (PAL). When a 30 mm (1.18") diameter PAL is positioned within a cavity a view of the cavity interior, extending from approximately fifty three degrees off the lens axis to about eighty six degrees off-axis and encompassing a full 360 degree surround of the axis, is mapped into a flat annular image. Figure 1, for example, shows the image obtained when a PAL is positioned along the axis of a cylindrical pipe, the interior surface of which is covered with a test pattern.

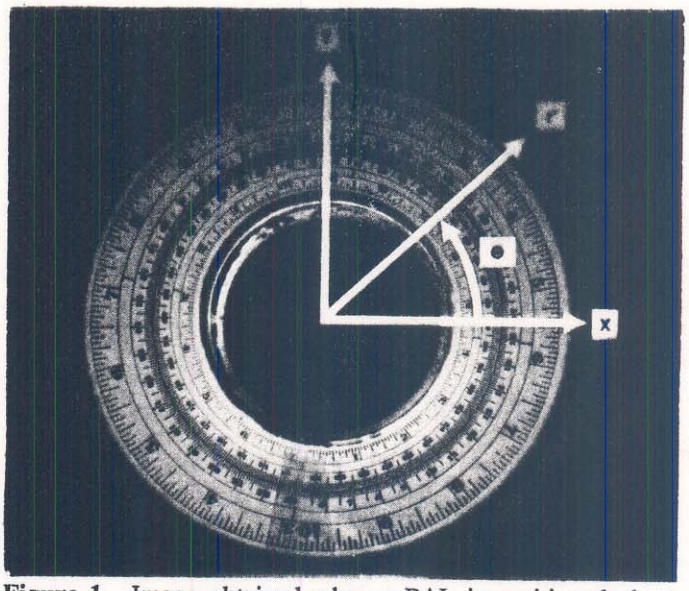

Figure 1. Image obtained when a PAL is positioned along the axis of a cylindrical pipe, the interior surface of which is covered with a test pattern. The coordinate system used to describe this image is superimposed.

An earlier paper on radial metrology described a device, called a radial profilometer, which was capable of contouring or measuring deflections on the inner surfaces of cavities.[2] Feasibility tests indicated that the measurement system could be designed so that profiling measurements were based on a linear calibration curve, and an analysis was presented which demonstrated that an entire cavity could be profiled simply by moving the profilometer through the cavity. Automated analysis was also discussed including the development of computer algorithms that transform the image into a form more easily interpreted by a human viewer.[3]

Since the profilometer used a line scan for profiling, it was necessary to move it through the cavity to obtain measurements over the original field of view. Unfortunately, such a procedure limits functional and real-time

capabilities. A subsequent paper suggested an alternative method for profiling in which measurements could be made by digitally recording and numerically correlating artificial speckle patterns projected onto the walls of a cavity.[4] In this case, the profilometer remains stationary during the measurement. The present paper further explores this approach and describes a series of tests conducted to illustrate this method.

Analysis

1. Movement of projected speckles as recorded in flat cylindrical perspective.

The PAL maps a cylindrical cavity onto a flat surface by flat cylindrical perspective (FCP), producing an annular image. The coordinate system used to analyze this image is shown superimposed on Figure 1. Figure 2, on the other hand, defines the cartesian (x,y,z) and cylindrical (r,θ,z) coordinate systems used to describe object space.

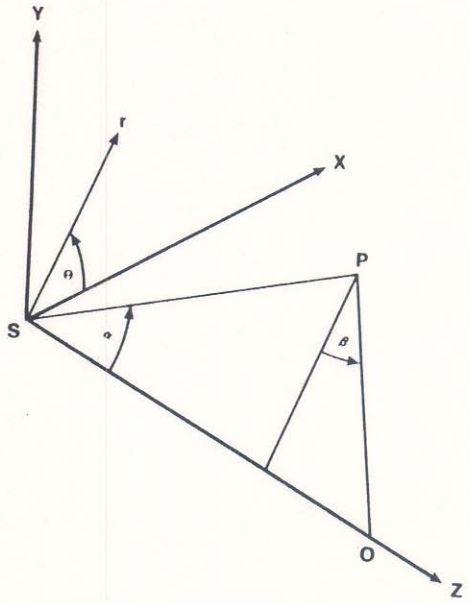

Figure 2. Cartesian (x,y,z) and cylindrical (r,θ,z) coordinate systems used to describe object space.

Referring to Figure 2, it is assumed that two opposing collinear PALs are aligned with their optical axes along the z-direction. Speckles, projected out from one PAL onto a reference standard or onto the cavity wall itself, fall on point P at an angle α, and the resulting speckle distribution is recorded through the second PAL at an angle β, measured with respect to a radial line lying in the r-z plane. When the surface moves through a displacement ξ along the radial direction r the projected image appears to shift along the z-direction through a displacement w. The radial displacement is given by

$$\xi = \frac{w}{\tan (90 - \alpha) + \tan \beta} \quad . \qquad (1)$$

The relationship between ξ and w changes over the field of view, since α and β vary from point to point.

The depth of field extends from the surface of the PAL out to infinity. However, the range over which measurements can be made depends on the geometry of the system, since the two PALs must be positioned so that the projected images of the initial and displaced speckle patterns are both captured in the image plane.

The speckle displacement along the z-direction is mapped into the image plane where a corresponding displacement ξ' occurs along the radial direction r'. The mapping of the displacement from the image plane to object space can be mathematically defined by a function g as

$$\xi = g(\xi'). \qquad (2)$$

This function would have to take into account the separation between the PALs, the radial distance between the test surface and the optical axis of the system, the design parameters of the PALs, and the mapping inherent in the optical transformation used to project the speckle pattern and create the PAL image. The following section illustrates that $g(\xi')$ can be experimentally determined using a calibration procedure.

2. Calibration of the measurement system.

One means of calibrating the PAL system is to use a circular pipe with its longitudinal axis initially positioned along the z-axis. When the pipe is translated along the x-axis through a displacement u, while keeping its longitudinal axis parallel to z,

$$r = u\cos\theta + (R^2 - u^2\sin^2\theta)^{1/2} \tag{3}$$

where R is the inner radius of the pipe.

Equation (3) can be derived using simple geometry, and defines the radial distance between the inner surface of the pipe and the optical axis of the measurement system for any angle θ. Equation (3) holds for any z-coordinate, since the cross section of the pipe is constant.

When the pipe is displaced along the x-axis, the projected speckles at different θ move through different amounts in a direction parallel to the z-axis. In the image plane, the speckles displace radially through a displacement ξ'. Since ξ' is a function of both θ and r', the PAL must be calibrated by assigning a specific value of r' to R and measuring the radial displacement as a function of θ. The calibration curve for the chosen value of r' is then established by plotting r [calculated on the basis of Equation (3)] versus r' [measured along radial lines on the image at different θ]. This procedure is repeated for different values of r' to obtain a family of calibration curves, from which the function in Equation (2) can be determined.

Once r is established for a known value of θ and r', the z-coordinate of the illuminated point can be calculated provided that α is known, since

$$z = \frac{w}{\sin\alpha} \ . \tag{4}$$

2. Displacement measurement by digital correlation.

Since the speckle pattern moves as the shape of the cavity changes, the variation in cavity shape can be measured by applying correlation techniques[5] to the speckle patterns obtained before and after the cavity shape is modified. The apparent speckle movement can be computed by numerically correlating small subsets (windows) extracted from each pattern. These shifts can be used to measure surface deflections or to contour the cavity with respect to a reference shape.

Digital correlation is a method of pattern recognition in which a small subset of an initial image is located in a second (deformed or displaced) image. A standard equation used to determine the correlation coefficient, ρ, for a window centered over location (m,n) in the displaced image is[6]

$$\rho(m,n) = \frac{\sum_x\sum_y[f(x,y) - \langle f\rangle][w(x-m,y-n) - \langle w\rangle]}{\{\sum_x\sum_y[f(x,y) - \langle f\rangle]^2 \sum_x\sum_y[w(x-m,y-n) - \langle w\rangle]^2\}^{1/2}} \tag{5}$$

where f(x,y) are the intensity values of the second image for those locations under the window values w(x,y) as the window is moved over a suitably chosen search range (x,y), $\langle f\rangle$ is the average intensity value of the region located under the window, and $\langle w\rangle$ is the average intensity value of the window. The maximum correlation value indicates the best match of the chosen subset from the initial image as located in the second image.

Experimental

An experiment was performed to illustrate the calibration procedure. Two 30 mm (1.18") diameter PALs, spaced at a distance of 47.63 mm (1.875") apart, were positioned with their optical axes aligned with the z-axis of the coordinate system shown in Figure 2. A circular pipe with an inner radius, R, equal to 69.85 mm (2.75") and a wall thickness of 3.0 mm (0.117"), was mounted on a kinematic stage and positioned midway between the PALs with its longitudinal axis also along z. A speckled slide was projected onto the inner wall of a 47.63 mm (1.875") long section of the pipe using a 35 mm projector and one of the PALs. The speckle

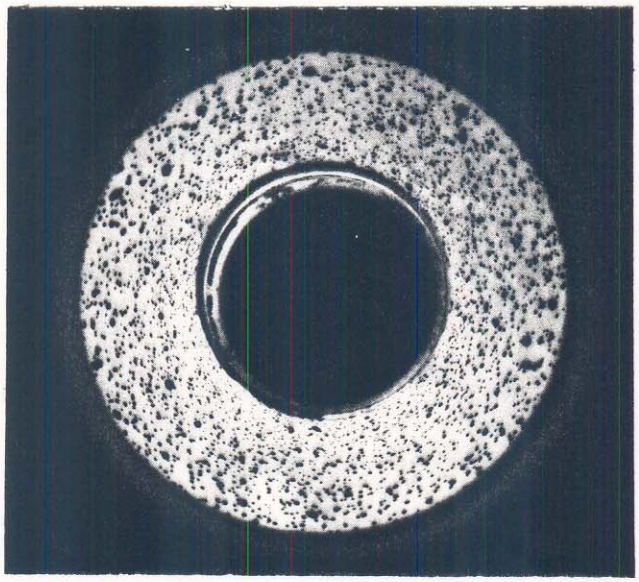

Figure 3. Image of the projected speckle pattern with the pipe located symmetrically with respect to the optical axis of the measurement system.

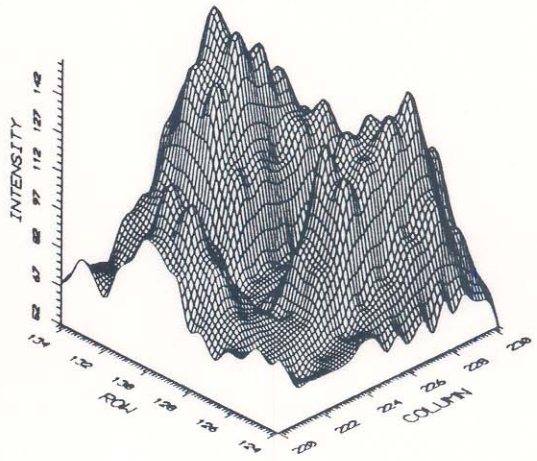

Figure 4. Intensity distribution in an 11 x 11 pixel window selected at r' = 100 pixels and θ = 0 (see Table 1).

pattern with the pipe in its initial position was captured through the second PAL, digitized using a CID camera, and stored as a digital array of 256 x 256 pixels with each pixel assigned a grey level ranging from 0 to 255. A second image was recorded after the pipe was translated along the x-axis, through a displacement u equal to 10.16 mm (0.4").

Figure 3 shows a photograph of the FCP image of the speckle pattern recorded through the PAL with the pipe in its original position. The image was digitized so that the center of the annulus, C, was located at pixel coordinates C(125,129). A subset with dimensions equal to 11 x 11 pixels was extracted from the image for each of the points used to calibrate the system. Figure 4, for example, shows the intensity distribution in a window selected at θ = 0 degrees with r' = 100 pixels. Ordinary correlation techniques were applied over a specified search region to determine the displacement of each subset in terms of pixel shift. The location of the displaced subset coincides with the point at which the correlation coefficient attains its maximum value. Figure 5, for example, shows an orthographic projection and the corresponding direct view of correlation coefficients obtained when the window shown in Figure 4 was compared with regions of equal dimensions contained in the image recorded with the pipe in its displaced position. In this case, correlation values were obtained over a 20 x 20 pixel search region surrounding the point. The location corresponding to the peak correlation of 0.780 is readily apparent, even though it was the lowest value measured for all of the points included in the calibration study. The displacement of ξ' = 9.65 pixels occurred along the radial line originating from point C.

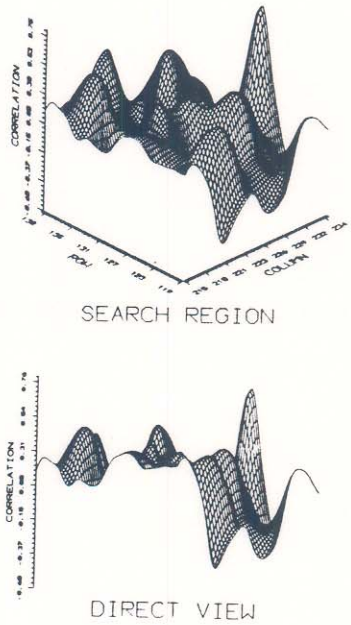

Figure 5. Orthographic projection and direct view of correlation coefficients obtained for the window shown in Figure 4 over a 20 x 20 pixel search region. The peak correlation is 0.780.

Table 1

θ	r(mm)	r'(pixels)	ρ	θ	r(mm)	r'(pixels)	ρ
0	80.06	109.65	0.780	180	59.74	89.20	0.877
10	79.88	108.88	0.871	190	59.87	88.86	0.914
20	79.36	108.90	0.912	200	60.27	89.83	0.938
30	78.51	108.57	0.896	210	60.92	90.94	0.941
40	77.38	107.24	0.941	220	61.81	91.88	0.948
50	76.00	105.96	0.951	230	62.93	93.03	0.920
60	74.42	104.85	0.961	240	64.26	94.68	0.934
70	72.72	103.01	0.958	250	65.77	95.89	0.947
80	70.94	100.77	0.975	260	67.42	97.10	0.961
90	69.16	99.40	0.971	270	69.16	99.20	0.959
100	67.42	97.24	0.914	280	70.94	100.66	0.986
110	65.77	95.88	0.954	290	72.72	102.69	0.983
120	64.26	94.70	0.942	300	74.42	104.61	0.962
130	62.93	92.89	0.893	310	76.00	105.78	0.933
140	61.81	91.44	0.905	320	77.38	107.58	0.956
150	60.92	90.86	0.903	330	78.51	108.61	0.838
160	60.27	89.80	0.914	340	79.36	108.87	0.963
170	59.87	88.92	0.940	350	79.88	108.73	0.852

Table 1 shows the results obtained for several other points initially located at r' = 100 pixels and taken at ten degree increments as θ ranged from 0 to 360 degrees. The calibration curve in Figure 6 was established by assigning the initial value of r' (100 pixels) to the original value of r (the inner radius of the pipe; namely, R = 69.9 mm) and plotting r [from Equation (3)] versus r' [100 + ξ'] for a displacement u of 10.16 mm (0.4"). The calibration is valid over a 20.32 mm (0.80") range where the value of r lies between 59.69 mm (2.35") and 80.01 mm (3.15"). In this range, the response is nearly linear. The slope of the curve represents the sensitivity s to which displacement is measured for the given value of r'. In Figure 6, for example, one pixel represents a radial displacement of approximately 1.00 mm (0.040"); therefore, s = 1 pixel/mm.

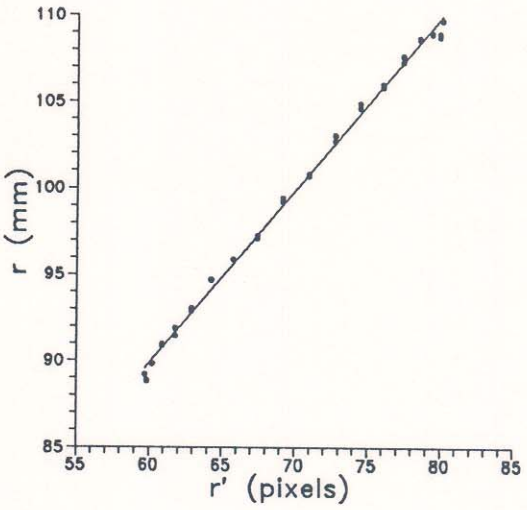

Figure 6. Calibration curve for r' = 100 pixels. Displacements range over 20.32 mm (0.08").

When speckles are projected onto the cavity wall, the pixel shift is measured in the image plane along radial lines originating from point C; a peak correlation value of 1.0 represents a perfect match. In general, the magnitude of the peak correlation decreases with increasing displacement. The predominant factor contributing to the progressive decrease in the peak correlation is attributed to the apparent change in the size of the speckles as they move in the FCP image. Speckles moving toward the center of the image are compressed while speckles moving away from the center are elongated. This may place a restriction on the range over which displacements can be measured, since peak correlations of less than 0.7 are generally suspect. Future research will focus on the development of computer algorithms to remove this distortion.

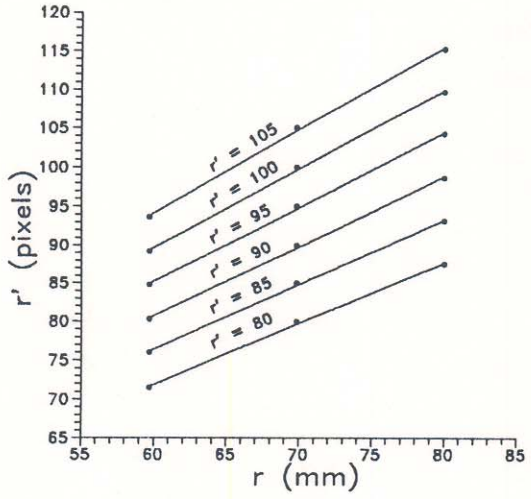

Figure 7. Calibration curves determined when r' is incremented by 5 pixels over the range from 80 to 110 pixels. Displacements range over 20.32 mm (0.80").

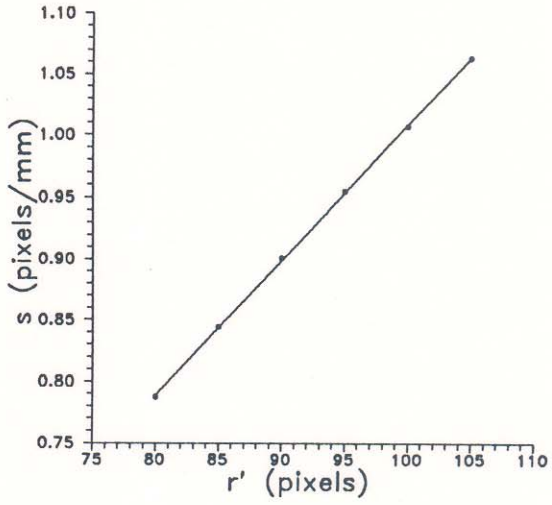

Figure 8. Plot of radial position (r') versus sensitivity (s).

The procedure for obtaining the calibration curve for r' = 100 pixels can be repeated for any r', since the cross section of the pipe is constant and radial displacements are independent of z. This allows a family of curves to be generated; Figure 7 shows calibration curves obtained as r' is incremented by 5 pixels over the range from 80 to 105 pixels. Each curve is nearly linear with a slightly different sensitivity. The linear response of the system allows these results to be graphically summarized in Figure 8, which shows a plot of r' versus s. Moreover, the function $g(\xi')$ can be defined in closed form by mathematically defining the curve in Figure 8, and then multiplying the displacement obtained from digital correlation by the reciprocal of the sensitivity. That is,

$$\xi = (0.011\ r' - 0.093)^{-1}\ \xi' \ . \tag{6}$$

The fact that $g(\xi')$ is independent of θ, and can be written in closed form may significantly simplify the calibration procedure for other PAL systems, provided that they display similar linear responses. The calibration could be performed simply by positioning a flat card parallel to the z-axis at a given θ. When the card is moved in the radial direction through a known displacement, the method of digital correlation could be applied along the corresponding radial line in the image plane to obtain the sensitivity as a function of r', thereby acquiring sufficient information to formulate an expression similar to that shown in Equation (6).

The results obtained from calibration were used to measure the deformation of the pipe when it was subjected to diametral compression. For this test, the pipe was returned to its original position, midway between the PALs with its longitudinal axis along z. The bottom of the pipe was rigidly supported by the kinematic stage at θ = 270 degrees, while a displacement of 12.58 mm (0.5") uniform in the z-direction was applied radially along the y-direction at θ = 90 degrees. Figure 9 shows the results of measuring ξ' for points initially located at r' = 100 pixels and taken at ten degree increments as θ ranged from 0 to 360 degrees. Figure 10 shows the deformation of the cross section. Results agree to within five percent of theory.[7]

The calibration procedure is sufficient to define r for a given value of θ and can be applied as illustrated to study deformations of a cavity when they are independent of z. In a more general case, the geometry of the cavity and the deformation will vary as a function of z, and Equation (4) must be used to completely analyze

the cavity. This, in turn, requires a complete description of how the PAL projects speckles onto the cavity wall. A subsequent paper will address this issue.

Conclusion

This paper describes a method in which measurements are made by digitally recording and numerically correlating artificial speckle patterns projected onto the walls of a cavity. The measurement system, which consists mainly of two collinear panoramic annular lenses, was calibrated using a section of circular pipe. Although the calibration procedure was tedious, the linear response of the system allowed families of calibration curves to be expressed in closed form. Moreover, results indicate that a relatively simple procedure can be applied to calibrate similar measurement systems.

Results obtained from a pipe under diametral compression indicate that deformations can be accurately measured, provided that both the cross section of the cavity and the deformations are constant along the length of the cavity. A subsequent paper will describe how speckles are projected by the panoramic annular lens, thereby providing the information required to analyze deformation in the more general case of a geometrically complex cavity.

Future plans for improving the method also include the design and construction of a practical measurement device, the development of computer algorithms to correct for speckle distortion in the acquired images, and refinements in the method used for calibrating the measurement system.

Acknowledgements

The authors wish to acknowledge support provided by the Physics Department at Marquette University, Milwaukee, Wisconsin, the College of Engineering at the University of Alabama in Huntsville, and the Applied Biophysics Laboratory at the Technical University in Budapest.

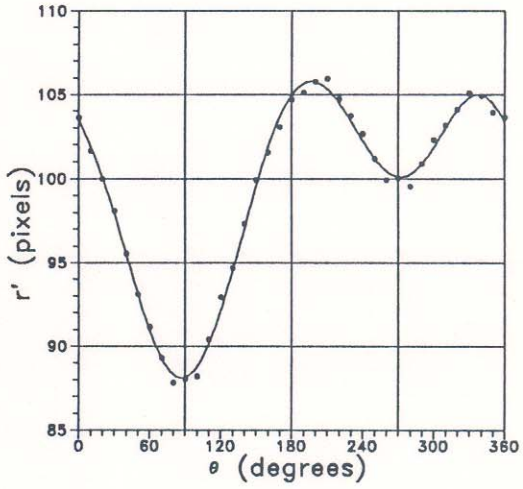

Figure 9. Radial deformation in the image plane for r' = 100 pixels of a pipe subjected to diametral compression.

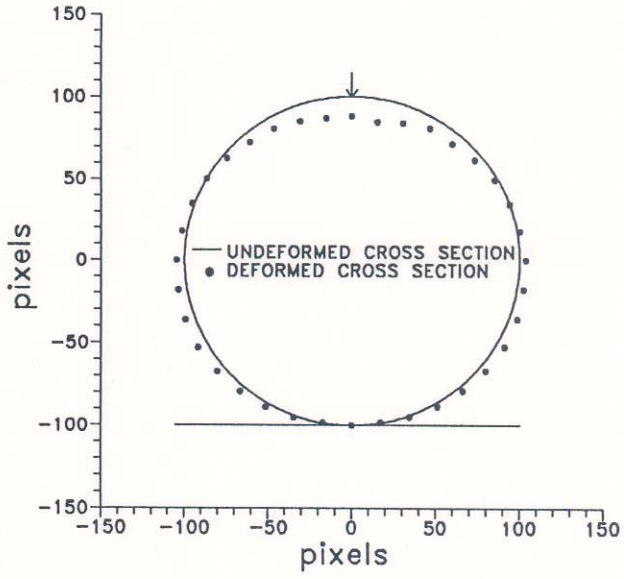

Figure 10. Deformed cross section of a pipe subjected to diametral compression.

References

1. Greguss, P., "The tube peeper: a new concept in endoscopy," Optics and Laser Technology 17, 41-45 (1985).

2. Gilbert, J.A., Greguss, P., Lehner, D.L., Lindner, J.L., "Radial profilometry," Proc. of the Joint BSSM/SEM International Conference on Advanced Strain Measurement Techniques, London, England, August 24-27,1987, Whittles Publishing, pp. 97-107.

3. Greguss, P., Gilbert, J.A., Matthys, D.R., Lehner, D.L., "Developments in radial metrology," Proc. of SPIE International Symposium on Optical Engineering and Industrial Sensing for Advanced Manufacturing Technologies, Vol. 954, Dearborn, Michigan, June 25-30, 1988, pp. 392-398.

4. Gilbert, J.A., Greguss, P., Matthys, D.R., Lehner, D.L., "Recent developments in radial metrology: a computer-based optical method for profiling cavities," Proc. of Optika '88, Third Int. Symp. on Modern Optics, Volume II, Budapest, Hungary, September 13-16, 1988, pp. 413-418.

5. Chu, T.C., Ranson, W.F., Sutton, M.A., Peters, W.H., "Applications of digital image correlation techniques to experimental mechanics," Experimental Mechanics 25, 232-244 (1985).

6. Gonzalez, R.C., Wintz, P., Digital Image Processing, 2nd edition, Addison-Wesley, 1987, p. 426.

7. Roark, R.J., Formulas for Stress and Strain, 3rd Edition, McGraw Hill, 1954, p. 156.